



Subsurface structures and conceptual hydrothermal model of the area lying between Quseir and Safaga area, Red Sea Coast, Egypt

Haby Salaheldin Mohamed¹

Received: 29 June 2020 / Accepted: 25 November 2020 / Published online: 8 January 2021
© The Author(s) 2021

Abstract

The study area is located in the Quseir–Safaga area of the Egyptian Red Sea Coast. This location considered one of the most promising areas for touristic villages depending on groundwater domestic uses as well as geothermal energy. The geothermal energy is considered one of the promising sources in the studied area. Nevertheless, few attempts have been carried out to evaluate the geothermal setting of the area. The present study aims to throw more light on studying the predominant structures in the area and their relation with geothermal manifestations, as well as defining the hydrothermal system type at the study area. Achieving this goal is dependent on using aeromagnetic data in the form of reduced to northern Pole (RTP) anomalies. These data were subjected to different techniques of processing and interpretation through both qualitative and quantitative analyses. Two-dimensional (2D) modeling of aeromagnetic data has been used to simulate the subsurface structure configuration along some selected profiles trending in NW-SE and E-W directions. In addition, a conceptual model of the hydrothermal system was built based on geophysical results of the aeromagnetic data analysis and processed numerically to obtain a 2D hydrothermal model that contains all simplifications and assumptions made on the conceptual model. The HYDROTHERM Interactive (HTI) program version 3 was used for two-dimensional simulation in the study area to study the temperature and pressure distributions beneath the study area. The results of the study showed that the depth to basement from the ground surface ranges from 20 to 1200 m. The hydrothermal simulation in the area indicated that the origin of thermal water is due to high heat flow and deep groundwater circulation controlled by structures in the subsurface reservoir. Under the thermal water, the water speeds up and flows through the fractures and faults. In general, the high heat flow in the Eastern Desert is associated with shallow basement depths. Thus, the modeled hydrothermal system is considered a dynamic type.

Keywords Aeromagnetic data · RTP · 2D modeling · Basement · Simulation · Conceptual model and hydrothermal system

Introduction

The Red Sea is characterized by a complex nature of geology and tectonic activity. Consequently, surface geology studies with geophysical surveys have been focused to study tectonic development where mechanisms of continental rifting, small ocean basin formation, and petroleum exploration occur. Moreover, the presence of a black shale with phosphate bed

in the Upper Cretaceous as well as deformation within the lithosphere and heat input from below the lithosphere and lateral conduction from the subsided Red Sea lithosphere contributed to the coastal anomaly leading to the production of the high observed heat flow values, up to 235 mW/m², in the Red Sea coastal zone (Martinez and Cochran 1989; Saleh et al. 2012). This means that the most promising areas for geothermal development in Egypt are located along the Red Sea Coast where temperature gradients of up to 45 °C/km are present (Abdel Zaher et al. 2014). Nevertheless, few attempts have been made to interpret the Red Sea coastal zone thermal anomaly. For example, Morgan et al. (1985) studied the basic mechanisms by which the high observed heat flow in the Red Sea coastal zone could be produced. Morgan and Swanberg (1979) indicated that there is little or no deep circulation of the surface water which means dry geothermal resources rather

Responsible Editor: Domenico M. Doronzo

✉ Haby Salaheldin Mohamed
habysalaheldin@yahoo.com; habysalaheldin@aun.edu.eg

¹ Geology Department, Faculty of Science, Assiut University, Assiut 71516, Egypt

than fluid-dominated systems from the eastern desert of Egypt. Given a decrease of water in the geothermal systems, and the generally arid nature of the region, probably the greatest use for geothermal resources in this area would be for seawater desalination to provide drinking water and irrigation water. Also, other authors studied the geothermal resources in different regions in Egypt, such as Abdel Zaher (2011a, b, 2014, and 2018) and Mohamed et al. (2015); Mohamed and Abdel Zaher (2019)). The geothermal waters in Egypt are used in direct heating, swimming pools, and greenhouses (Lashin 2015 and Elbarbary et al. 2018). Generally, the hottest springs are on the east bank of the Gulf of Suez: Uyun Musa (48 °C) and 'Ain Hammam Faraoun (70 °C). Additional warm springs are located on both banks of the Gulf of Suez. The eastern desert of Egypt, in particular the coastal region bordering the Red Sea, has a heat flow above normal ($< 72 \text{ mW/m}^2$) and thus a certain geothermal potential, although only a thermal well (Umm Kharga: 35.8 °C) could be localized. In the large oases of the western desert (Kharga, Dakhla, Farafra, and Bahariya), the regional temperature gradient is small ($< 20 \text{ }^\circ\text{C/km}$), but many of the wells develop deep artesian aquifers and produce large amounts of water in the range 35–43 °C. Such wells form a low temperature geothermal resource (Swanberg et al. 1983). Swanberg et al. (1988) classified the groundwater in Egypt chemically into four types: MgCl_2 , CaCl_2 , NaSO_4 , and NaHCO_3 . MgCl_2 waters are represented by the Red Sea and Mediterranean Sea, CaCl_2 waters are confined to the coastal areas of the Eastern Desert and Sinai, NaSO_4 waters are the most common water types in Egypt, while NaHCO_3 waters are represented by the River Nile.

This study investigates the Quseir–Safaga area in the Central Eastern Desert of Egypt. This area is located on the western side of the Red Sea coast between Quseir–Safaga at Lat. 25° 50', 26° 67' N and Long. 33° 45', 34° 25' E (Fig. 1). This location is considered one of the most promising areas for touristic activities depending on groundwater for domestic uses as well as non-conventional sources of energy. Geothermal energy is considered a promising source in the under study.

Most previous work in the study area was focused on studying the surface geology with no concern as to geothermal accuracies. The only geophysical work carried out in the area is that conducted by Salem et al. (2005) from which the general structures were defined in the subsurface in the Quseir area by using aeromagnetic data. Khalil and McClay (2001) described extensional fault-related folding in the northwestern Red Sea. Minerals and inorganic trace elements have been evaluated as the content in the black shale deposits of Duwi Formation in some phosphate mines exposed in the Safaga–Quseir area (Ghanem et al. 2016). Shalaby et al. (2006), Fowler et al. (2006, 2007), Andresen et al. (2008), Abd El-Wahed (2008, 2010), and Abd El-Wahed and Abu Anbar

(2009) have supplied important information about the tectonic activity of the Egyptian Eastern Desert. Gaafar et al. (2016) used the integrated carbon X-ray spectrometric data, X-ray analysis, and HPGe X-ray spectrometer data to investigate the radioactive zones in the Safaga–Quseir area. Youssef et al. (2009) used GIS tools to evaluate the geomorphological hazards to delimit the most susceptible areas for flashfloods and mass wasting in the Red Sea area between Safaga and Quseir, Egypt. Abdelmaksoud and El-Haddad (2019) applied shallow seismic refraction measurements along three profiles using direct and reverse shooting to investigate the near-surface geological conditions and to solve the major problems of the lack of sufficient and safe water supply of Wadi El-Nakheil to the west of the Quseir district along the Egyptian Red Sea Coast.

The purposes of the current study are (1) to provide detailed subsurface geological structure information in the study area (tectonic framework) and (2) develop a numerical-conceptual model of the hydrothermal system beneath the study area. To achieve these aims, geophysical data in the form of magnetic field reduced-to-the-pole maps are used. The conceptual geothermal model for the area was first constructed based on geological and geophysical results. Then, the conceptual model was processed numerically to obtain a two-dimensional (2D) computer model that contains all the simplifications and assumptions made in the conceptual model. The HYDROTHERM Interactive (HTI) program version 3.1.1 was used for the 2D simulations in the area to study the characteristics of the heat sources below this area (modified after Hayba and Ingebritsen 1994).

Geology and structural setting

Morphologically, the study area is bounded by Wadi Quseir el Qudeim, Wadi Safaga, Wadi Abu Shegeila on the north, Wadi Nakheil and Wadi Beda el Atshan on the west, Wadi el Isewid on the south, and by the Red Sea in the east. The area is characterized by a flat coastal plain with uplifted, west-dipping plateaus of middle to late Tertiary sediments related to the Red Sea and an elevated inland region. The inland region has a rugged topography, with a relief of several hundred meters, which was developed on strongly deformed Precambrian basement and local steeply inclined fault blocks from Cretaceous to Eocene platform sediments.

Geologically, many authors have described in detail the stratigraphy of the area between Quseir and Safaga such as Barron and Hume (1902), Ball (1913), Youssef (1957), Faris and Hassan (1959), Akaad and Dardir (1966), Akaad and Noweir (1969), Abd El Razik (1967, 1972), Gindy et al. (1973, 1976), and El-Gaby et al. (1990). The stratigraphic units in the area between Safaga and Quseir can be divided into three rock units (Fig. 2). The rock units are arranged from

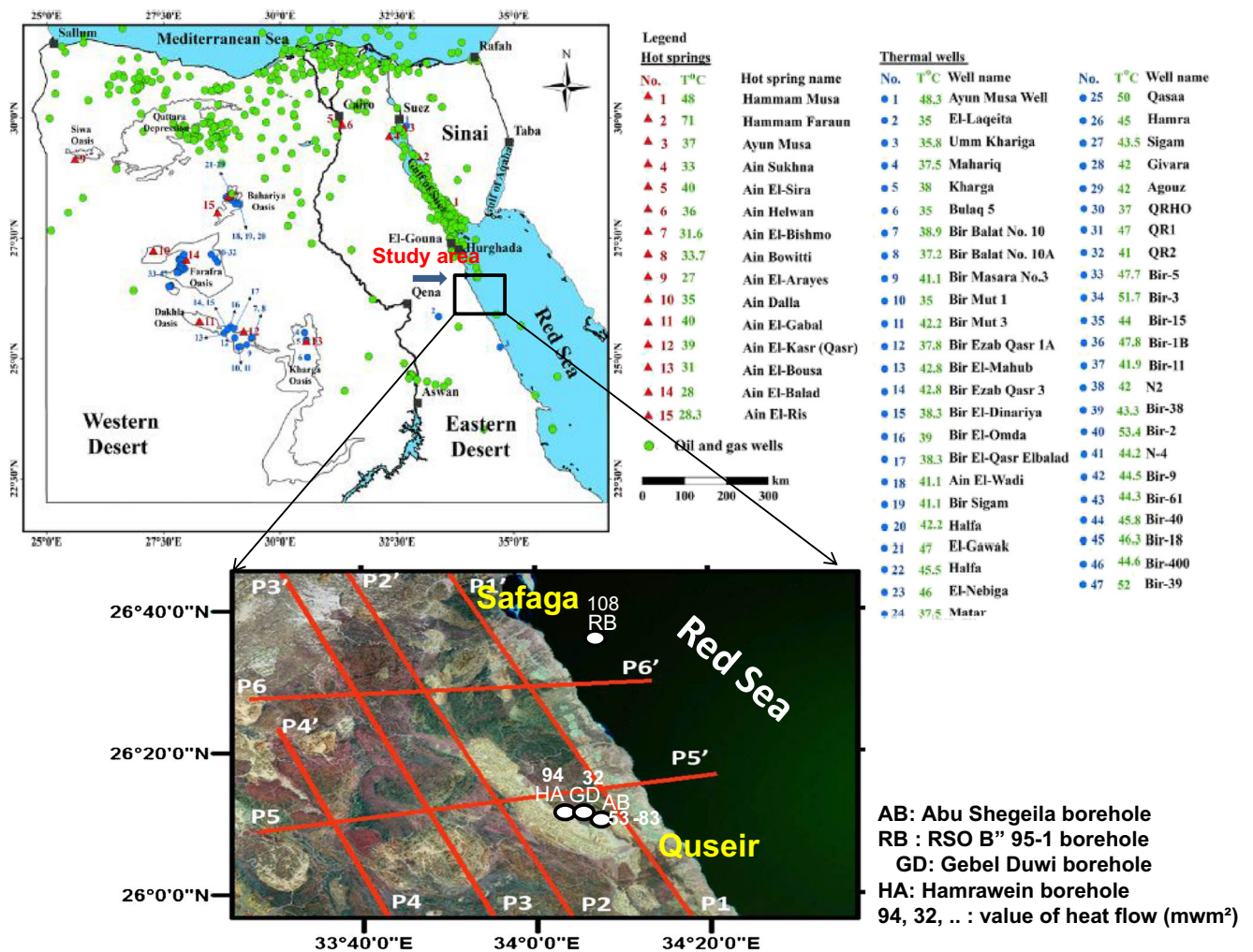


Fig. 1 Map of Egypt showing the location of the main geothermal manifestations, including hot springs and thermal water wells. The figure shows the location the study area and hinterland shown by

Landsat TM scene (MDA Federal (2004) and red lines indicate the location of selected profiles used for 2D magnetic forward modeling

base to top (Fig. 2): basement (metavolcanics, meta-sediments, and granitoid intrusive (Said 1990)), pre-rift sediments (Mesozoic-Cenozoic), and synchronous-rift sediments (Late Oligocene-Miocene to Recent). Hume (1935), Akaad and El Ramly (1960), El Shazly (1964), El-Ramly et al. (1970), El-Ramly (1972), and El-Gaby et al. (1984) showed that the basement rocks are essentially composed of pan-African assemblages comprised of gneisses, migmatites, metasediments, ophiolitic melanges, metavolcanics, mafic intrusions, granodiorite, molasse sediments, younger volcanics, post-tectonic granites, and trachyte plugs and sheets. The Precambrian units are unconformably overlain by the Phanerozoic sediments, especially in the southeastern (Miocene) parts of the mapped area. The pre-rift strata (Late Cretaceous to Middle Eocene) are unconformably on the basement. The sediments of the pre-rift strata are represented by massive beds of Nubian Sandstone at the lower part (Khalil and McClay 2009). The

Duwi, Dakhla, Quseir, and Esna Formations lie over the Nubian Sandstone (Abd El Razik 1967; Issawi et al. 1969). The Thebes Formation consists of limestones and cherty limestones and represents the uppermost pre-rift strata of the Lower to Middle Eocene. The syn-rift strata represent from Late Oligocene to Recent age (Heath et al. 1998). The Nakheil and Ranga Formations at the lowermost syn-rift strata are coarse-grained clastics which underlay the Um Mahra, Sayateen, and Abu Dabbab formations (evaporite (gypsum) deposits). From the late Miocene to Recent syn-rift, carbonates, reefs, and clastics were above evaporation products in the coastal outcrops (Montenant et al. 1988).

Structurally, the study area was subjected to different tectonic movements, leading to a complex series of normal faults with different trends, half-grabens, and folds. These trends are interpreted by many authors to lie in the directions NE-SW, NW-SE, NNE-SSW, ENE-SWS, WNW-ENE, N-S, and E-W

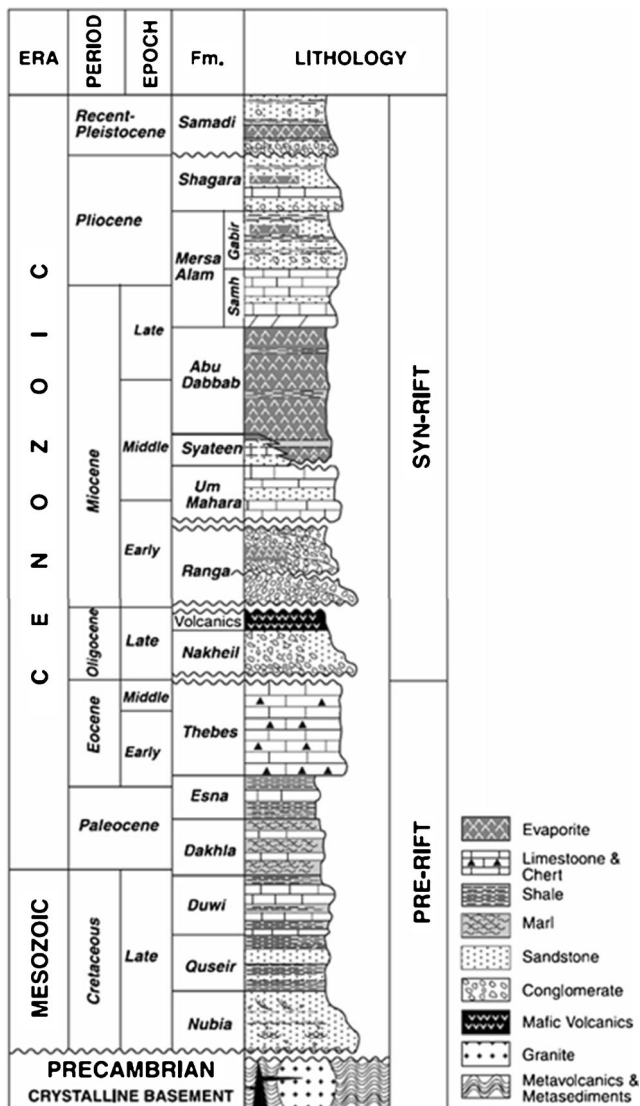


Fig. 2 Stratigraphic section of the northwestern Red Sea rift system (Khalil and McClay 2002)

(Garson and Krs 1976; Garson and Shalaby 1976; Valentine 1985; Moustafa 1997; Younes and McClay 2001; Khalil and McClay 2002, 2009; Amer et al. 2012a, b; Metawi 2017) (Fig. 3). The main faults and folds have an important role in estimating the shape of the structural setting and framework of the area. The main faults are El Nakheil, Atshan, Queih–Abu Shegeily, Um El Huwyat, and West Gebel Duwi Fault. On the other hand, the main folds are trending NNW-SSE and NW-SE, into which the Cretaceous–Eocene series were involved during the Late Eocene and Oligocene times. The El Nakheil, Atshan, El Anz, Um El Huwyat Syncline, and Mohammed Rabah Syncline folds are contacted with some faults such as the Nakheil, Mohammed Rabah, Um El Huwyat, and Atshan faults. Beadnell (1924) pointed that there are several anticlines in the post-Eocene strata in the area between El Quseir and Wadi Ranga. On the eastern side, the area is intersected by the WNW-ESE sinistral strike-slip fault

and the NNW-SSE shear zone. This shear zone dips toward the WSW by an angle of about 65° (Greene 1984). Younes and McClay (2001) indicated that the study area is characterized by Precambrian structural features of the Arabo-Nubian shield, which is a system of linear, deep-seated shear zones which were considered left lateral northwest oriented faults and shear zones (Hamrawien shear zone) (Abuzeid 1988). Also, there are several dikes occurring through the basement of the study area.

Studies on the northwestern part of the Red Sea showed complex structures that mainly consist of two main fault systems with several NW- and WNW-trending half-graben basins (Younes and McClay 2002). The first type is the Borders Fault system forming the western margin of the rift and causes the juxtaposition of the pre-rift strata and the syn-rift Nakheil Formation against the Precambrian basement in the footwall of the extensional faults. Meanwhile, the second type is the Coastal Fault system that makes the pre- and syn-rift Miocene strata juxtaposed against the Precambrian basement. The Coastal Fault system tends to trend toward the NW direction, which is sub-parallel to the coastline. The Border Fault system is more complicated than the coastal one and is strongly segmented with two dominant faults: the Nakheil Fault and the Hamadat Fault. This fault system has a trend that tends to the rift trend. Both fault systems mainly consist of NW, WNW, and NS fault segments, which form a zigzag fault pattern that beats fault blocks.

Methodology and data acquisition

Aeromagnetic data

The magnetic method is considered the best tool in geophysical exploration to identify the location and properties of magnetic rocks, in addition to detecting subsurface structures by means of disturbances that are reduced at the surface in the earth's magnetic field. Aeromagnetic data was applied to study the general image of the subsurface structures of the study area and achieve the main goal of the study through the analysis and interpretation of this data. The data was provided by the Egyptian General Petroleum Corporation (E.G.P.C.) as part of the Mineral and Petroleum and Groundwater assessment program in 1980 in the form of reduced-to-the-pole (RTP) aeromagnetic map (Fig. 4a).

Processing and interpretation of the aeromagnetic data

A fast Fourier transform was performed on the RTP magnetic data to create the energy spectrum curve and to define the residual (shallow) and regional (deep) sources. Low-pass and high-pass filters and tilt angle processing techniques were

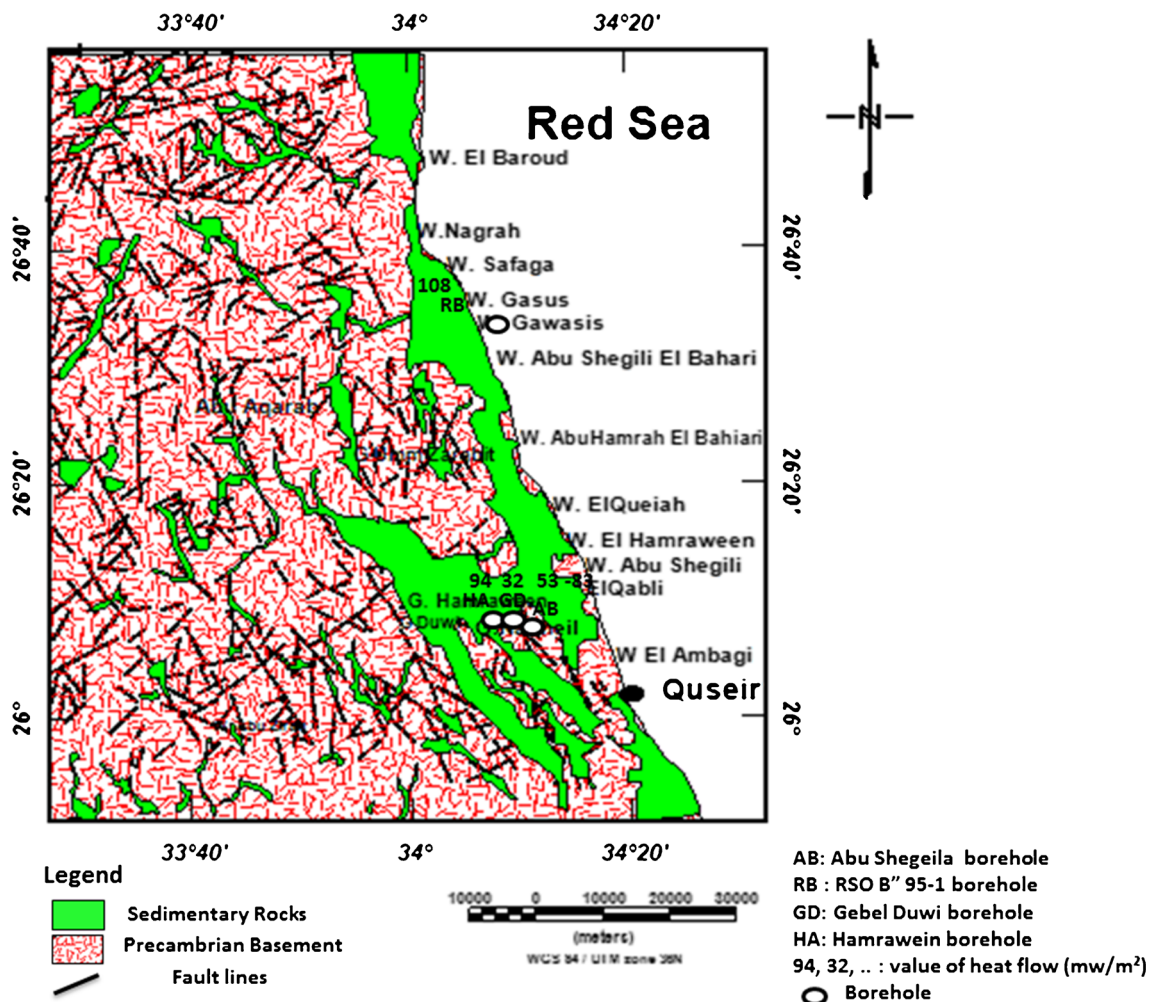


Fig. 3 Simplified geological and structural map of the study area (modified after CONOCO 1987 and Abdel Moneim 2005)

also applied to determine the vertical and inclined lithological contacts of structural contacts or lines. In addition, the data were interpreted qualitatively and quantitatively. The qualitative interpretation of the RTP aeromagnetic data was focused on the description of the distribution and extension of the anomalies, while the quantitative interpretation was concentrated on the determination of the basement depth (consequently the thickness of the sedimentary cover). The following is a brief qualitative description of the RTP aeromagnetic, low-pass, high-pass, and tilt derivative maps.

The natural lithology of the study area reflects changes in the intensity of aeromagnetic data. The area could be divided into three types of rock: Late Proterozoic rocks composed of the Ophiolite Group (serpentine, metagabbro, metavolcanics, and metamorphosed shelf sediments); Cretaceous rocks composed from Taref Sandstone, varicolored shale, and siltstone; and Cenozoic rocks, from marl and limestone. These rocks can be seen on the aeromagnetic maps as high and low anomalies according to their type and magnetic susceptibility.

The RTP aeromagnetic map (Fig. 4a) of the study area includes different shapes of the magnetic anomalies from elongated to oval and some anomalies were nearly circular. Other magnetic anomalies are irregular, which can be attributed to lateral inhomogeneities in magnetic properties. Most of these magnetic anomalies' patterns are aligned along NW-SE, but some magnetic anomalies have E-W and NE-SW directions. Also, positive and negative magnetic anomaly values appear on the RTP map and vary from -300 up to +350 nT. The positive anomalies are very common in the area due to outcrops of basement rocks which have high magnetic susceptibility. These anomalies are notable in Gabal Umm Shagir and Bir Umm Fawakir at the southern parts and Gabal Semna, Bir Abu Mareiwat, and Gabal Abu Aqarab in the central parts and different parts in the north where Ophiolitic Serpentine, older granite, and metavolcanic rocks are present. On the other side, the negative magnetic anomalies are found in Gabal Hamrawein, Gabal Duwi, Gabal Nakheil, Gabal Umm Kugura, Gabal Umm Zarabit, Gabal

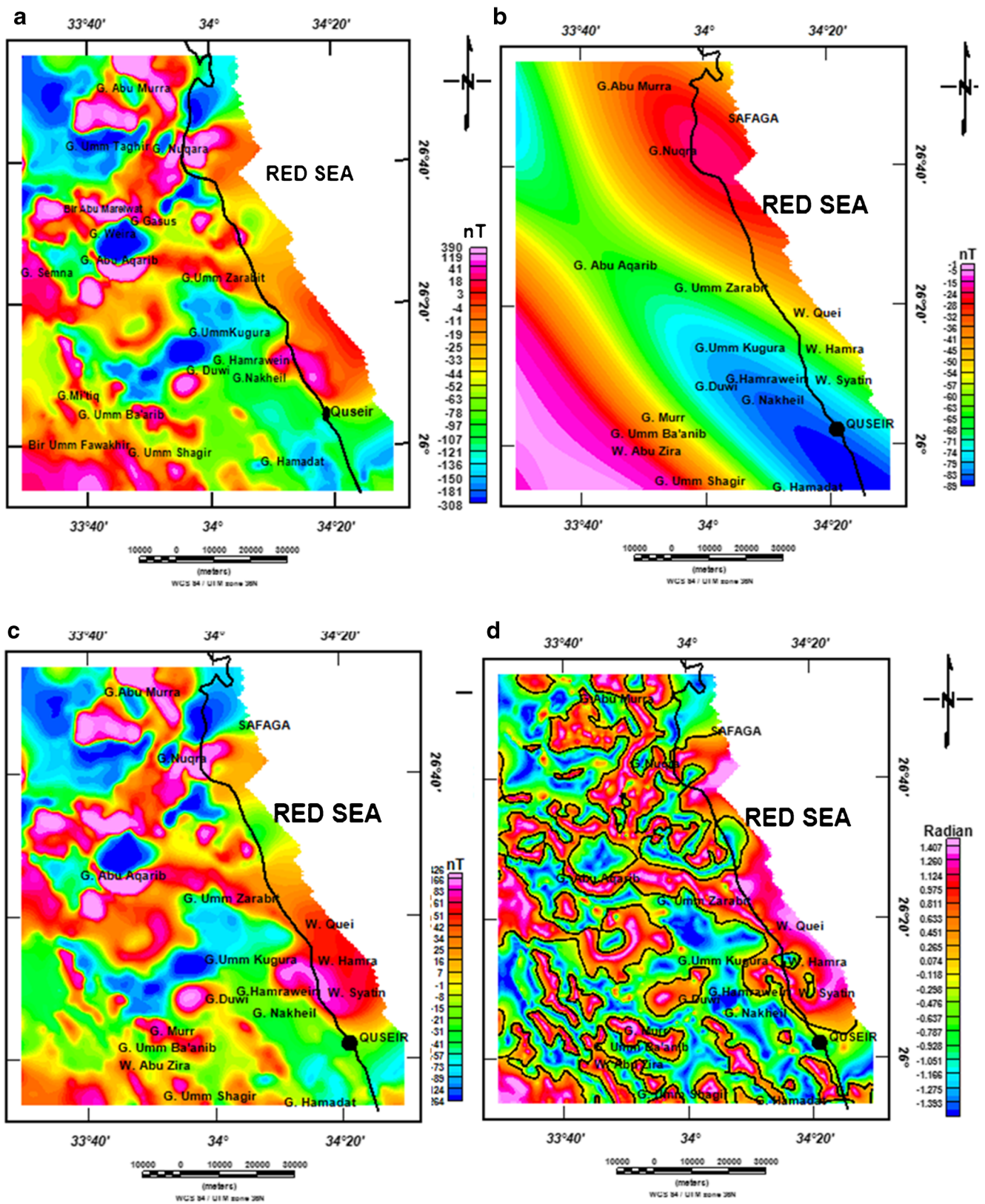


Fig. 4 (a) RTP aeromagnetic map of study area; (b) low-pass filtered regional RTP map (cut-off wavenumber = 0.015 cycle/km); (c) high-pass filtered residual RTP map (cutoff wavenumber = 0.015 cycle/km); (d) tilt derivative map of RTP aeromagnetic data

Um Taghir, and Gabal Abu Murra, where younger granite, metasediment, and Cretaceous rocks are present.

The low- and high-pass filters with cutoff 0.015 cycle/km were applied on the RTP data of the studied area, using Geosoft Oasis Montaj 8.3 (2014) for obtaining the regional and residual components. The low-pass filter map (Fig. 4b) indicates the regional anomaly which reflects the deep-seated and regional structures. All regional anomalies are in a linear pattern extending in a NW-SE direction. These anomalies in the NW-SE direction are a characteristic of the deep fault systems. On the other hand, the high-pass filter map (Fig. 4c) presents structural features of intermediate and shallow depths. Both the high-pass filter map and the RTP aeromagnetic map have a good resemblance to each other and lead to the same interpretation.

A tilt derivative filter (TDR) was applied to the RTP aeromagnetic data to enhance weak anomalies, otherwise overshadowed by stronger structures (Salem et al. 2007). The result of this filter is presented as a contour map shown in Fig. 4d. The map shows that the TDR values range between -1.4 and 1.3 rad. These values refer to the localization of the edges of structures. According to Miller and Singh (1994), the positive anomalies' values are over the sources and are negative outside the source region. The zero contours on the map indicate the location of source edges which are illustrated by the black lines. The major anomaly pattern is aligned along the NW-SE and E-W directions which present the predominating trend in the area. These directions are concordant with the main structural units in the area.

Magnetic trends

Interpretation of aeromagnetic data into tectonic information is the most important thing, where the major structural features on the surface of the basement that influence the overlying sedimentary cover play an important role in tectonic interpretation of a certain area. In addition, the magnetic trend patterns can be used to define magnetic ones' provinces, which in turn reflect tectonic provinces (Affleck 1963; and Hall 1964). Gay (1972) defined the aeromagnetic lineaments as a disruption in the contour pattern. These disturbances are caused by the juxtaposition to blocks of rocks of varying composition (varying magnetic susceptibility) at different locations along opposite sides of the lineament. This leads to the conclusion that most of the common geologic causes of an aeromagnetic lineament may be due to faulting. So, the Gay technique (1972) was used for the detection of fault trends from the RTP map. Meanwhile, in the low- and high-pass filter maps, tilt angle maps' faults are traced by applying the Rosenbach consideration (Rosenbach 1953) that considered the zero contour lines as traces of faults. Figure 5 shows the magnetic fault trends traced from the aeromagnetic maps of the study area which were determined from the zero contour lines as traces of faults.

Forward modeling

The forward modeling process transforms the variations reflected by aeromagnetic data in an area of study, as shown by the RTP aeromagnetic, regional residual, and tilt derivative maps to a convenient subsurface geological setting. In addition, the forward modeling process calculates and estimates the basement surface depth and the outline of structural framework of the area. The two 2D modeling of aeromagnetic data was used as a quantitative interpretation by GM-SYS through Oasis Montaj 8.3 (2014).

Six profiles were drawn on the RTP aeromagnetic map. Four profiles were selected in the SE-NW direction (P1-P1', P2-P2', P3-P3' and P4-P4'). These profiles are parallel to the Red Sea coast. The other two profiles were selected to extend in the W-E direction (P5-P5' and P6-P6') as shown in Fig. 1. The magnetic susceptibility values which were used were assumed according to the classification of the rock units in the area and their susceptibilities. Consequently, in each profile model, magnetic susceptibility values were tried until a reasonable fit between observed and calculated magnetic anomalies was achieved. So, the magnetic susceptibility ranges used for modeling in the study area are from 0.015 to 0.038 in cgs units for the basement rocks (Table 1). The magnetic susceptibility values of rocks which are used and assumed in the study are according to what is published in Parasnis (1986), Sharma (1986), and Telford et al. (1990). Figure 6 shows the result of the 2D geologic models which were obtained from the aeromagnetic data.

Geothermal resources in the area

The main objective of this study is to shed more light on the origin of the thermal water (hydrothermal system) in the area between Quseir and Safaga. Generally, resources of groundwater in the Eastern Desert are limited and represented by shallow alluvial and fractured basement aquifers in the southern parts and sandstone and carbonate aquifers in the northern parts. In addition, the main sources for the direct recharge of these are seasonal rainfall events and surface water runoff. El-Baz (1995), Abdel Moneim (2005), Sultan et al. (2008), Ruelleu et al. (2010), Sultan et al. (2011), and Amer et al. (2012a, 2013) indicated that the water present in the confined aquifers is paleowater, probably accumulated during hotter climatic periods of the Early Holocene and Pleistocene. Recent geothermal studies have concentrated on the Central Eastern Desert by many authors (Ravat et al. 2011; Abdel Zaher et al. 2011a, b, 2012; Saleh et al. 2012; Lashin 2013; Atef et al. 2016; Chandrasekharam et al. 2016). These studies have provided important information about high geothermal gradient and heat flow values that appear to be concentrated in

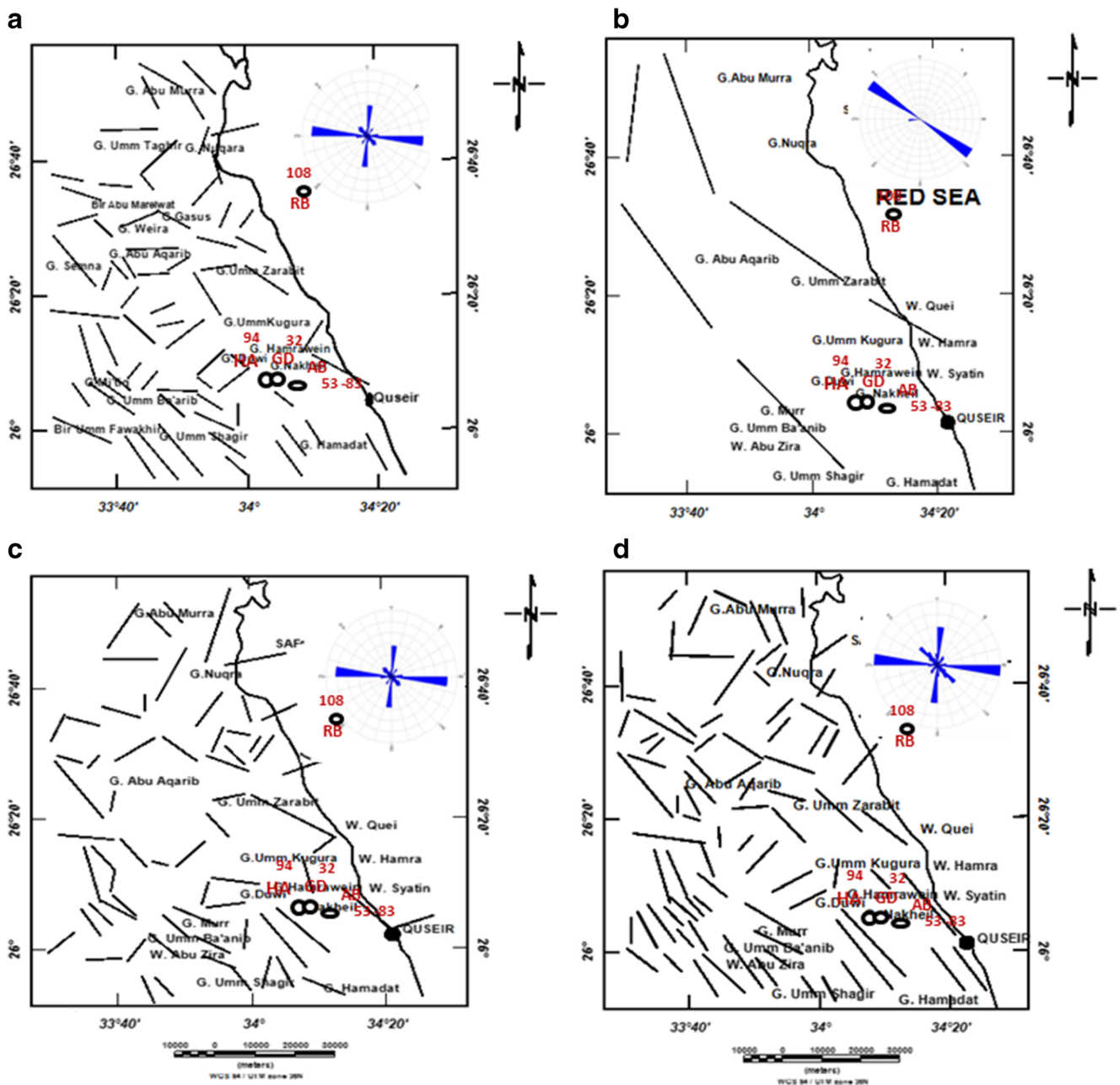


Fig. 5 Magnetic structure lineaments traced from the aeromagnetic maps of the study area that reflect the structure lines and the corresponding azimuth frequency diagram. (a) RTP aeromagnetic map; (b) low-pass filtered regional RTP map; (c) high-pass filtered residual RTP map; (d) tilt gradient map

the coastal zone of the Red Sea. Some geothermal resources along the Eastern Desert region adjacent to the Red Sea occur in the form of hydrothermal systems within the radiogenic granites (Chandrasekharam et al. 2016). Other geothermal resources have high heat flow with non-radiogenic granites in the Eastern Desert restricted to the coastal zone such as Abu Shegeila. The geothermal gradient measured at Abu Shegeila ranges from 30 to 50 mK/m at respective depths of 65–160 and 175–235 m due to a conductivity contrast. The high gradient of 50mK/m indicates a high heat flow of 105 mW/m²

similar to the mean of 111 mW/m² reported for the Red Sea margin (Girdler and Evans 1977). The high gradient values in the shallow sedimentary cover at Abu Shegeila borehole do appear to be a representative of the deeper thermal regime.

In the present study, the conceptual model of the hydrothermal system was focused on the thermal water in the Abu Shegeila area where the ground surface is near to the regional water table and thermal water emerges from Oligocene sandstone acting as the water-bearing formation in Wadi El-Nakheil at 35- to 65-m depth.

Table 1 The magnetic susceptibility values in cgs for the basement rocks used in the 2D forward modeling

Types of Basement rocks	Magnetic susceptibility values
	0.006
	0.009
	0.015
	0.02
	0.017 : 0.019
	0.022
	0.025
	0.038
	0.034

The colors indicate different types of basement rocks

Conceptual hydrothermal model

Generally, conceptual models of geothermal systems are spatial representations of the physical visibility of the system and are presented by 2D cross sections. Also, a conceptual model represents a qualitative model based on geological information (from surface mapping and analysis of subsurface data) as well as geochemical data.

In the present study, the conceptual model of the hydrothermal system was assumed based on the information extracted from the geological and geophysical data (aeromagnetic data). This information indicated that the hotter rocks close to the surface (tectonic uplifting) heat groundwater are found to be trapped in porous rock or water running along fractured rock surfaces and faults. Such fractures allow the formation of discharging conduits for meteoric water ascending from depth after being heated and mixed with other water types (Fig. 7). From this conceptual model, a 2D hydrothermal model is presented in the following parts. The basic mechanism of the geothermal systems in the study area is governed by fluid

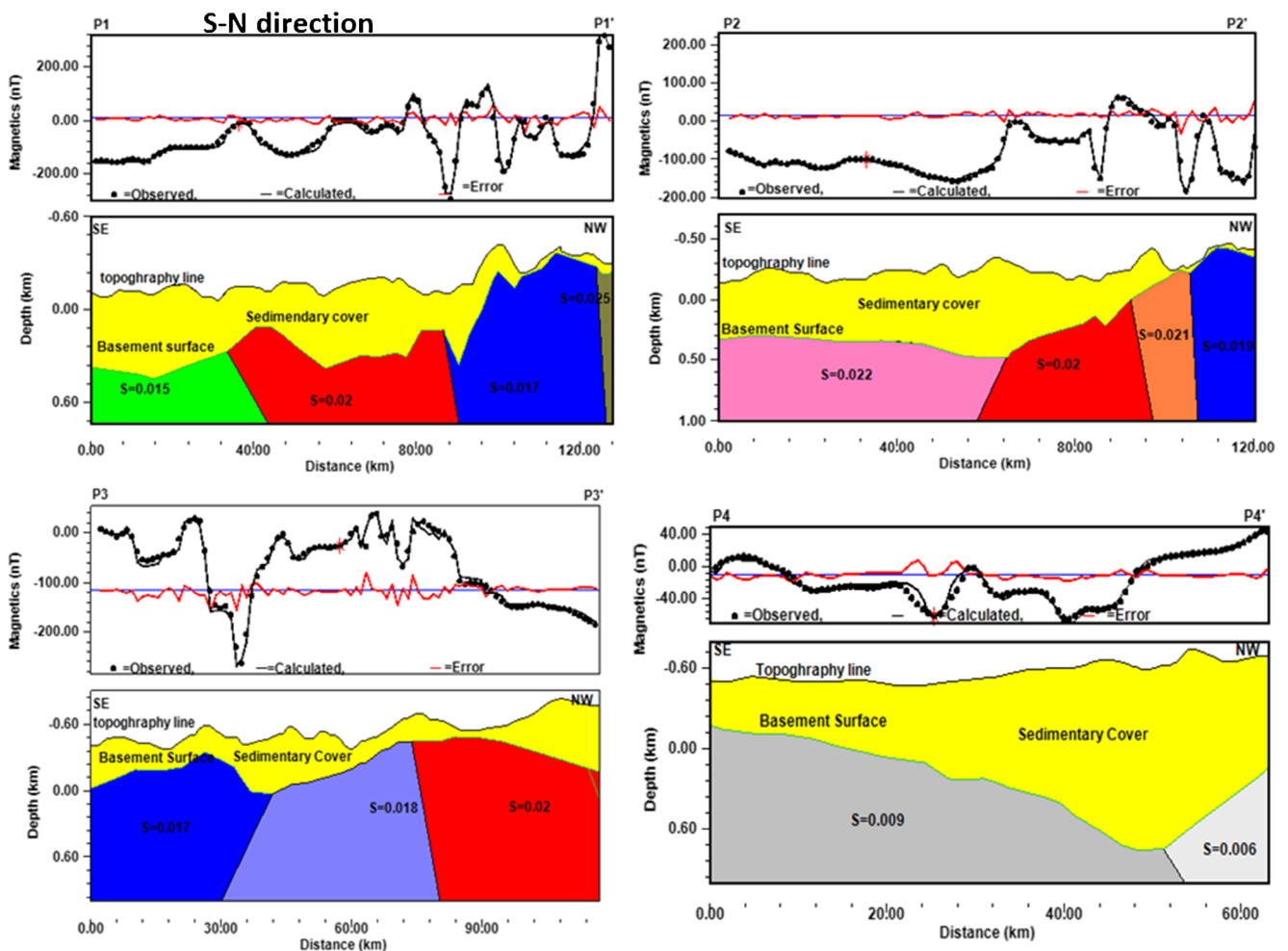


Fig. 6 2D forward aeromagnetic models along profile P1, P2, P3, P4, P5, and P6 which extend in the W-E and S-N directions; the locations of these profiles are shown in Fig. 1

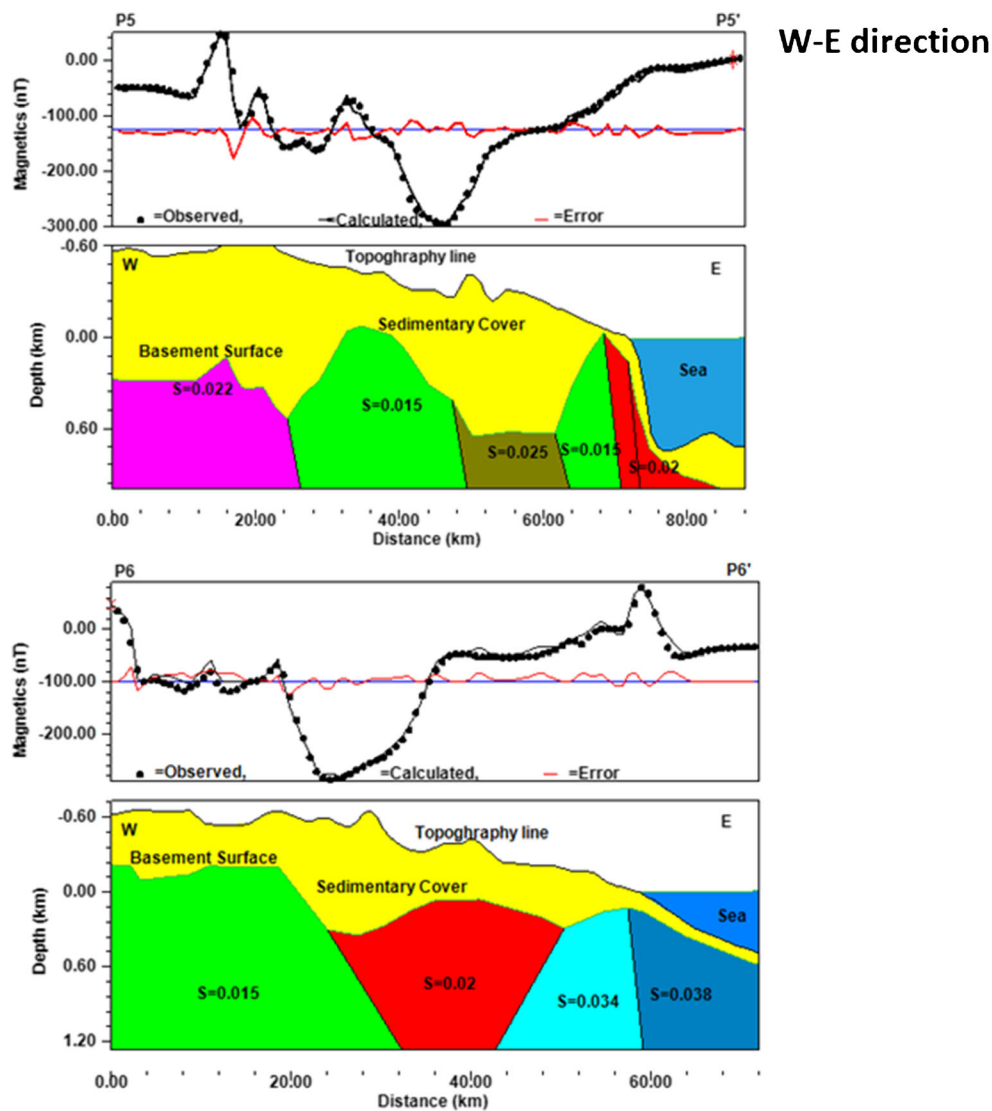


Fig. 6 continued.

convection. The convection system occurs due to the heating fluid of lower density that rises to be replaced by colder fluid of high density, coming from the margins of the system.

2D numerical hydrothermal model

The purpose of numerical modeling is to produce a computer model that includes all simplifications and assumptions made at the conceptual model and reflects essential features of the phenomenon considered or simulates a real system. In the present study, the model represents the evolution of hydrothermal circulation along a cross section in the study area with a bottom heat source of 200 °C. The HYDROTHERM Interactive (HTI) program version 3 was used to simulate groundwater flow and heat transport in a porous medium below the selected section to study the characteristics of the heat sources below this area.

The following is a brief summary of the setup of the 2D hydrothermal model (Hayba and Ingebritsen 1994) and the initial conditions of the numerical simulation such as temperature gradient, pressure gradient, boundary conditions for temperature, and pressure.

The presented model domain of the area was the first step in the simulation. The domain is the area of fluid flow and heat transfer simulation. For the current study, the shape of the simulation domain is symmetrically rectangular with 120 km length and a width of 1.0 km (Fig. 8). Drawing in the rock units was the second step to build the model. Three layers were used in the model with different physical properties: sedimentary, basement rocks, and fractures. The fracture zone was assumed to be a simple porous medium with different hydraulic properties that are due to faults and fractures within the basement layer. Rock properties for these layers such as porosity, permeability, conductivity, density, and specific heat are kept constant during the

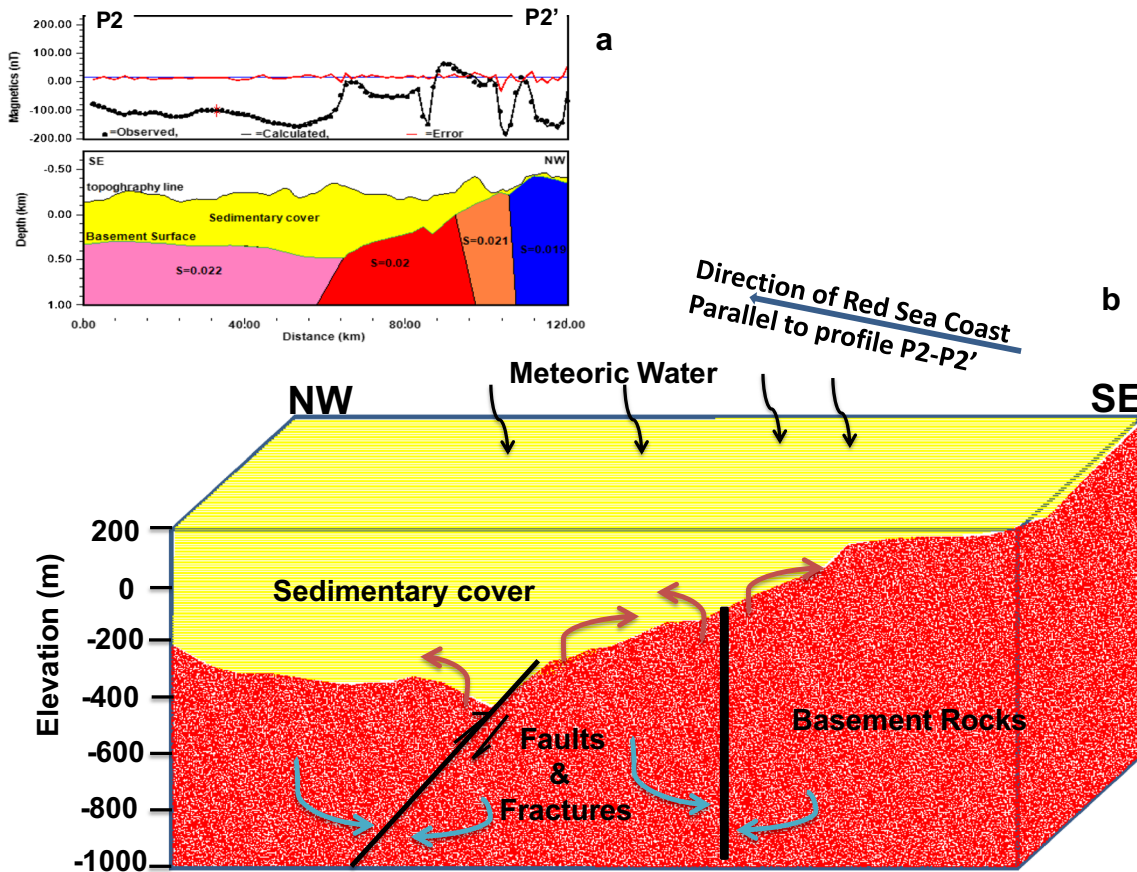


Fig. 7 (a) 2D magnetic model along profile P2-P2; (b) schematic diagrams show the conceptual model of the hydrothermal system in the study area (especially at Abu Shegeila) along profile P2-P2

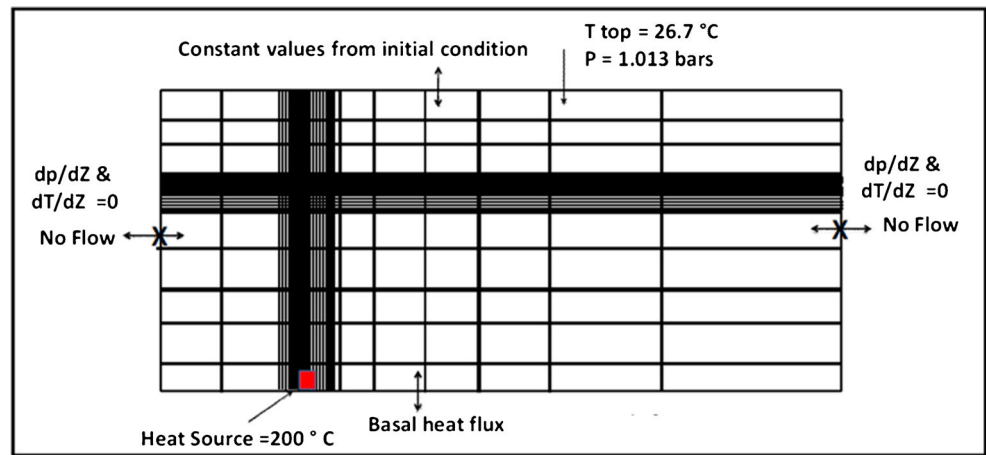
simulation. These properties are displayed in Table 2. The values of physical rock properties are assumed in the present study according to the previous studies carried by Morgan et al. (1983, 1985), Meneisy (1990), and El-Nouby and Ahmed (2007). The estimation of fracture porosity and permeability values as absolute values is difficult. The subsurface circulation of geothermal fluids through the fractures leads to chemical reactions, mineral dissolution, and precipitation, which affect the fracture porosity and permeability. So, in the present study, different values of fracture permeability were applied in the simulation model to reach a steady state for the fracture permeability. This study found that the fracture permeability value must be not more than 10^{-10} cm^2 .

The third step was gridding. The HYDROTHERM simulator uses a finite-difference method to discretize the governing equations. Spatial discretization of the simulation region is accomplished using a mesh or a grid of rectangular cells. The grid in the program may be edited either graphically in the drawing area or using the table in the grid dialog window with uniform dimensions in each of the two coordinate directions, where the number of cell columns and cell rows comprising the grid are specified. The rectangular boundary of the initial grid contained the polygon of the simulation domain. In the present study, the special discretization is rather coarse with 20 grid blocks along the profile direction and 14 blocks in vertical direction. The width of grid block

Table 2 Physical rock properties applied in the hydrothermal model for each layer

Name	Density (g/cm ³)	Porosity (%)	Permeability (cm ²)	Thermal conductivity (W/mk)	Heat capacity (J/kg.k)
Sedimentary rocks	2.4	10	10^{-13}	1.8	800
Basement rocks	2.67	5	10^{-15}	2.6	750
Fracture	1.5	30	10^{-10}	0.5	1000
Heat source	Temperature (°C)		Mass flow (kg/s)		
	200		60		

Fig. 8 Setup of the model domain showing the construction of grid, boundary condition, and the location of heat source



dimensions varies between 2.0 km and 8.0 km, with the highest resolution applied near to the fractured uplifted area and low resolution at the buffering area. Vertically, the model extends from + 500 m ASL to 1.0 km BSL.

A simulation period is a time span during which the boundary conditions and sources remain constant. So, numerical experiments were carried out for 100,000 and one million years simulation in the current study with time step of 0.01 years.

Fig. 9 Basement depth map as interpreted from the 2D aeromagnetic modeling

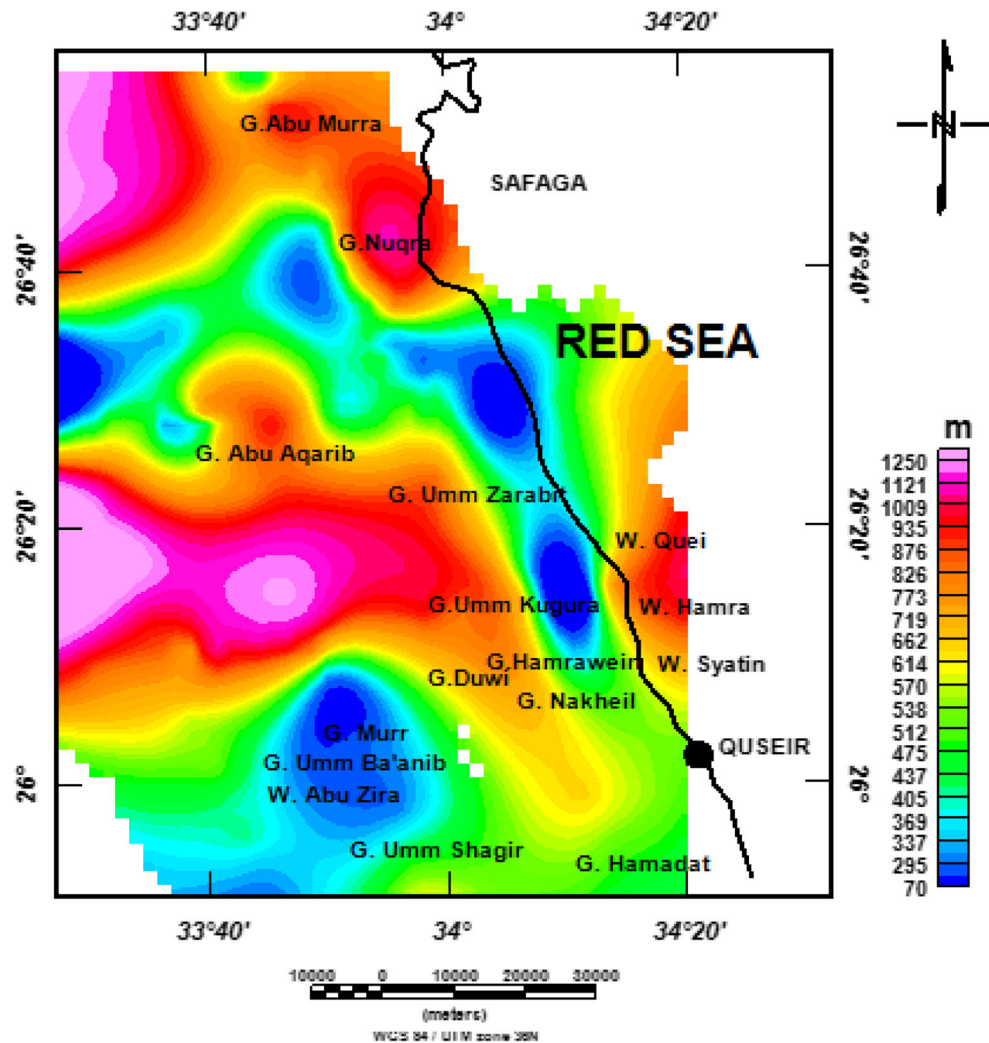
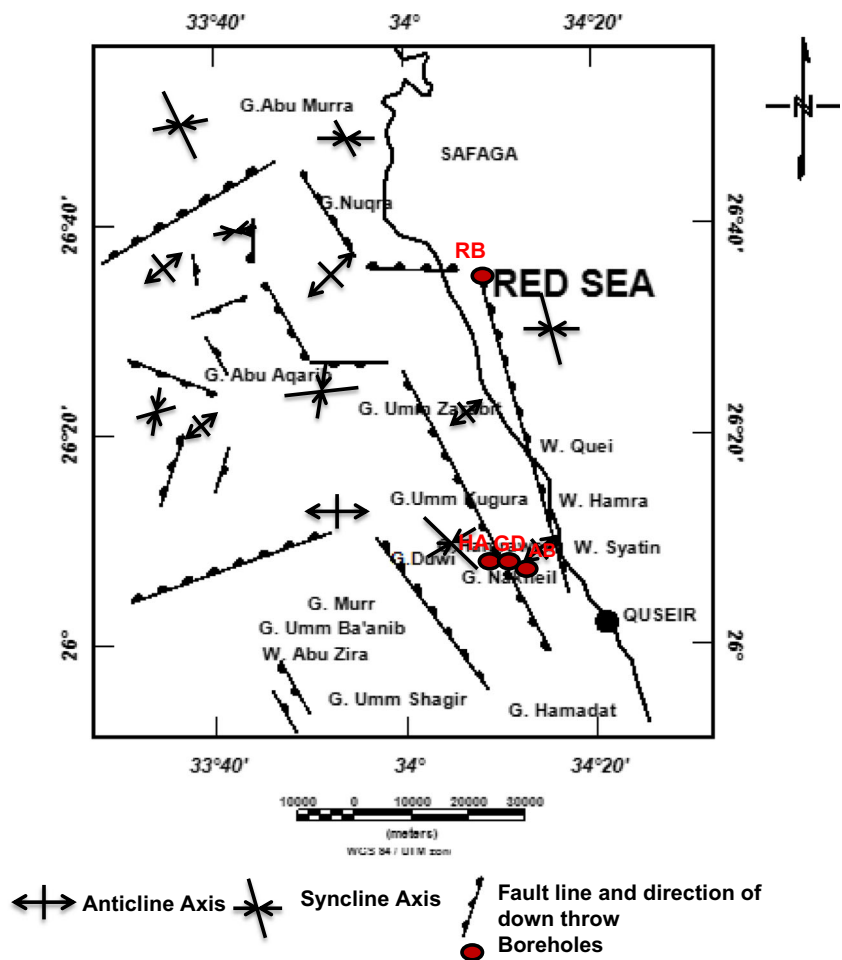


Fig. 10 Basement tectonic map of the study area, as interpreted from the depth to basement map and the corresponding azimuth frequency diagram



The lateral boundaries' conditions are set as insulating and impermeable. Also, temperature and pressure gradients do not change at the sides of the box indicating no flow. The upper (land surface) boundary is maintained at a constant temperature of 26.7 °C and a pressure of 1.013 bars to represent ambient water table conditions. The heat flow values were found to range between 100 and 150 mW/m² for the study area. Thus, the basal boundary was made impermeable with a constant heat flux of 100 to 160 mW/m² toward the fracture zones as a boundary condition constraint. On the other hand, a head source was assumed and located at the bottom of the model at 200 °C with a mass flow of 60 kg/s. Finally, the HTI postprocessor was run to display simulation results including the fluid mass and thermal energy balance errors at the bottom of the display area. They indicate the accuracy of the numerical solutions to the flow and thermal transport equations.

Results and discussion

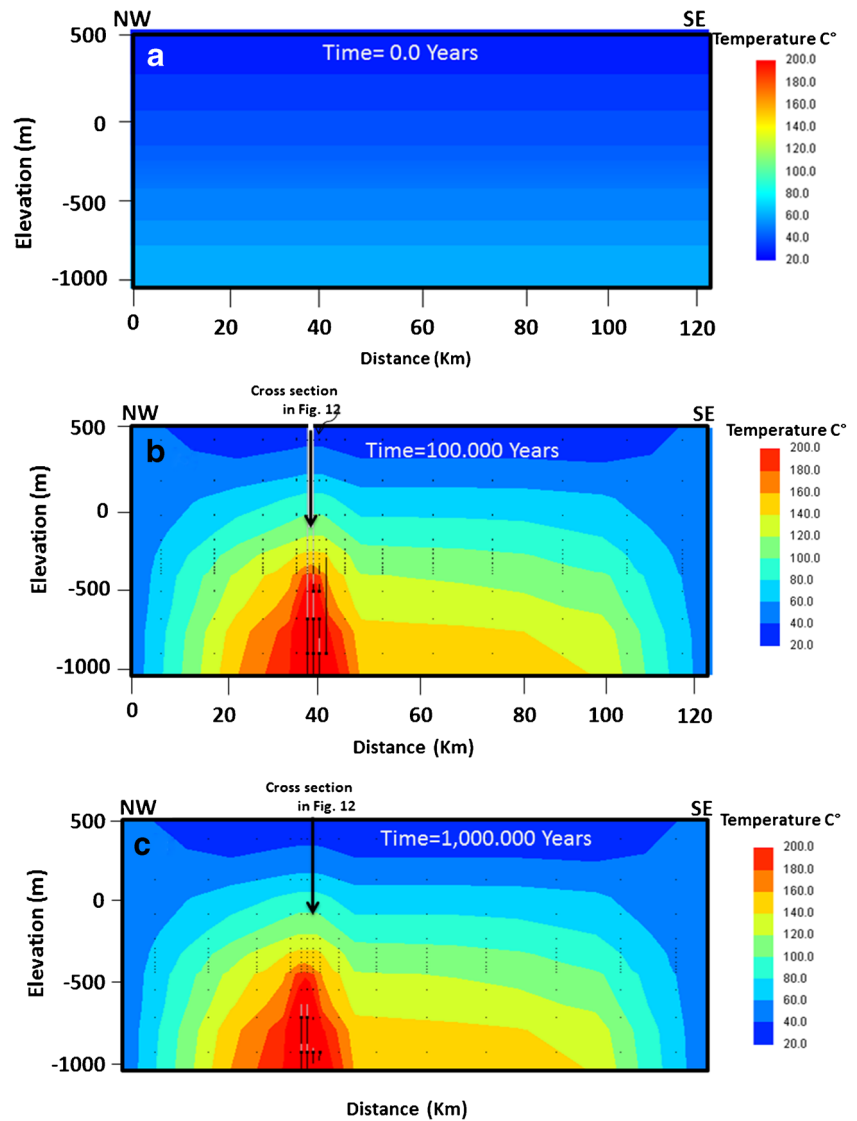
The qualitative interpretation of the RTP aeromagnetic anomaly map of the study area and its derivative (Fig. 4) revealed

that major positive and negative anomalies have NW-SE extension as pointing to the major structure trend in the study area. The centers of these anomalies referred to basic and acidic rocks, respectively. However, the boundary between these positive and negative anomalies could represent a geological contact or faults.

The magnetic trends in the study area were deduced from the RTP map and its derivative based on Gay technique (1972). The trend analysis of the aeromagnetic maps can be shown in Fig. 5. It is clear that the most predominant trends are the NW-SE, E-W, and NE-SW trends. The NW-SE trend is continuous to deeper subsurface levels and considered the regional trend in the study area.

The quantitative interpretation was focused on determination of the basement depth (consequently the thickness of the sedimentary cover) at parts of the study area in which the basement is buried beneath sedimentary rocks. This was carried out using 2D modeling of aeromagnetic data along some selected profiles in the area trending in the NW-SE and E-W directions (Fig. 7). The results obtained from the 2D models were integrated in constructing a basement topographic map (Fig. 9).

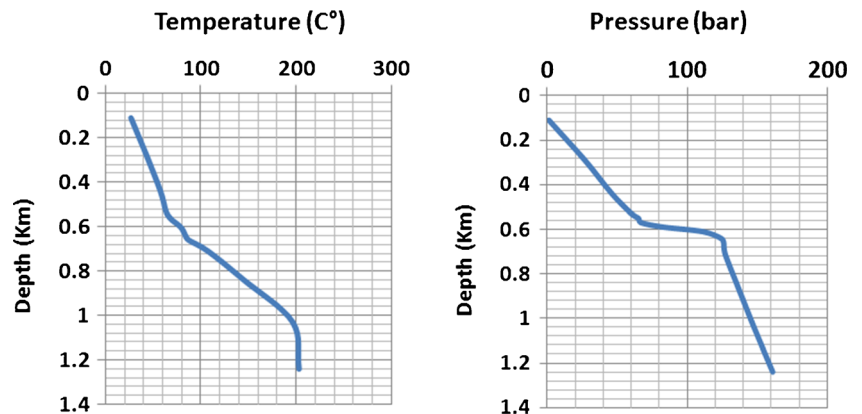
Fig. 11 Temperature distribution and water flux pattern on S-N section across Abu Shegeila of the HTI postprocessor; (a) an initial model for temperature field (without run); (b) temperature field after run simulation at time = 100,000 year; white vertical line refers to the cross section in Fig. 12



This map exhibits the depth to the basement surface in the area under consideration from the earth surface, ranging between 20 and 1250 m (Fig. 9). The depth to basement is deeper in the central and eastern parts near the Red Sea coast,

reaching to 1200 m, while it varies from 400 to 700 m at the Wadi El Nakheil. In other areas, the basement rocks are shallower with a depth of 20 to 150 m. However, the basement rocks outcrop (uplifted blocks) at Gabal Murr, Umm Ba'anib,

Fig. 12 Vertical cross section indicates the distribution of temperature and pressure with depths along the fracture zone. The location of the cross section is shown in Fig. 11



Murra, and Nuqra in the southern and northern parts of the study area. From the depth to basement map, a structural contour map of the basement surface was prepared (Fig. 10). The map shows the main structural trends which affected the basement surface and continued upward into the sedimentary cover extending in ENE-WSW, E-W, NW-SE, and NNW-SSE directions. These structural trends resulted in different uplifts and basins. On the eastern, southern, and northern sides of the area, the major NW fault is forming major uplifts in the form of anticlines while at the central and southeastern parts, the faults formed basins or synclines extending in the E-W and NW directions.

The results of the hydrothermal simulation at the area are presented in Fig. 11. In case of initial conditions, spatial distributions with depth for temperature can be defined by specifying the value as a function of location at the top of the global mesh and specifying the gradient with depth. Thus, the background temperature and pressure distributions of the study area can be calculated due to a homogeneous distribution of the subsurface temperatures (Fig. 11a). Also, the steady-state simulation (including a fracture zone) was run for up to 100,000 years and 1,000,000 years and the final result can be seen in Fig. 11b and c. The results of this simulation indicate that the temperature increased at shallow depth below the fracture zone to reach up to 160 °C (Fig. 12). Also, the temperature and pressure distributions in the model have not changed significantly over time.

The model indicates that the origin of thermal water in this area is due to high heat flow and groundwater circulation controlled by structures in the subsurface reservoir. The water velocity increased below the thermal water and flowed upward through the fractures and faults where the circulation of the groundwater causes transfer of the heat upwards by advective processes, i.e., the transport of heat by a moving medium. But also note that the heat can be transferred by conduction processes, i.e., the transport of heat through a stationary medium by vibration of atoms. The high heat flow is also associated with shallow basement depths. Thus, the modeled hydrothermal system is considered a dynamic type and the source of the geothermal potential is due to tectonic local uplift of hotter rocks causing deep fluid circulation through the faults on the surface of the basement rock. Along the fractures, the temperature increases rapidly and, in the model, reached 160 °C at a depth of less than 1.0 km, while the pressure increases gradually.

Also, the geothermal gradient can be estimated from the numerical model along the fracture. For example, the temperature value concluded from the numerical model is 30 °C at a depth of 100 m with geothermal gradient of 30 °C/km. These values are identical to the Abu Shegeila borehole, where the geothermal gradient measured at Abu Shegeila ranged from 30 to 50 °C/km at respective depths 65–160 and 175–235 m due to a conductivity contrast.

Conclusion

The main conclusions and the most important outcomes from the present study can be listed as:

- 1- The study area is affected by sets of fault systems trending in the NNW-SSE, NW-SE, and NE-SW directions.
- 2 The depth to basement varies from one place to another. It ranges from 400 to 700 m in the southeastern part at Wadi El Nakheil, while in the central and eastern parts it reaches 1200 m. However, the basement rocks are shallower with a depth of 20 to 150 m where outcrops are uplifted blocks in Gabal Murr, Umm Ba'anib, Murra, and Nuqra at the southern and northern parts of the study area.
- 3 The basement structural map shows that the NW trend is considered the dominant older fault systems in the study area.
- 4 Normal faults/contacts which are observed within the basement represent ideal sites for geothermal manifestations (structural control on the geothermal gradients).
- 5 The origin of thermal water in the Quseir area is due to high heat flow (at Abu Shegeila) and deep groundwater circulation controlled by structures in the subsurface reservoir. The high heat flow is associated with shallow basement depths.
- 6 The modeled hydrothermal system is considered a dynamic type and the source of geothermal potential is due to tectonic local uplift of hotter rocks causing deep fluid circulation through the faults on the surface of the basement rock that are likely related to the opening of the Red Sea.

Open Access This article is licensed under a Creative Commons Attribution 4.0 International License, which permits use, sharing, adaptation, distribution and reproduction in any medium or format, as long as you give appropriate credit to the original author(s) and the source, provide a link to the Creative Commons licence, and indicate if changes were made. The images or other third party material in this article are included in the article's Creative Commons licence, unless indicated otherwise in a credit line to the material. If material is not included in the article's Creative Commons licence and your intended use is not permitted by statutory regulation or exceeds the permitted use, you will need to obtain permission directly from the copyright holder. To view a copy of this licence, visit <http://creativecommons.org/licenses/by/4.0/>.

References

- Abd El Razik TM (1967) Stratigraphy of the sedimentary cover of Anz-Atshan-south Duwi district: Bull. Fae. Sci., Cairo University, no. 41, p. 153–176
- Abd El Razik TM (1972) Comparative studies on the upper Cretaceous – early Paleocene sediments of the Red Sea coast, Nile Valley and Western Desert, Egypt. 8th Arab petrol. Congr., Algiers, Paper (B-3), 23pp
- Abd El-Wahed MA (2008) Thrusting and transpressional shearing in the pan-African nappe southwest El-Sibai core complex, central Eastern Desert, Egypt. *J Afr Earth Sci* 50:16–36

- Abd El-Wahed MA (2010) The role of the Najd fault system in the tectonic evolution of the Hammamat molasse sediments, Eastern Desert, Egypt. *Arab J Geosci* 3:1–26. <https://doi.org/10.1007/s12517-008-0030-0>
- Abd El-Wahed MA, Abu Anbar MM (2009) Syn-oblique convergent and extensional deformation and metamorphism in the Neoproterozoic rocks along Wadi Fatira shear zone, northern Eastern Desert, Egypt. *Arab J Geosci* 2:29–52. <https://doi.org/10.1007/s12517-008-0016-y>
- Abdel Moneim AA (2005) Overview of the geomorphological and hydrological characteristics of the Eastern Desert of Egypt. *J Hydrol* 13:416–425
- Abdel Zaher M, Saibi H, El Nouby M, Ghamry E, Ehara S (2011a) A preliminary regional geothermal assessment of the Gulf of Suez, Egypt. *J Afr Earth Sci* 60:117–132
- Abdel Zaher M, Saibi H, Nishijima J, Mesbah H, Fujimitsu Y, Ehara S (2011b) Exploration and assessment of the geothermal resources in the Hammam Faraun hot spring, Sinai Peninsula, Egypt. *J Asian Earth Sci* 45:256–267
- Abdel Zaher M, Saibi H, Ehara S (2012) Geochemical and stable isotopic studies of Gulf of Suez's hot springs, Egypt. *Chin J Geochem* 1: 120–127
- Abdel Zaher M, Saadi NM, Watanabek K (2014) Geological applications potential of DEM, ETM, and gravity data in arid and semi-arid regions with special reference to South Western Desert, Egypt. *Arab J Geosci* 7(5):1705–1716
- Abdel Zaher M, Saibi H, Mansour K, Khalil A, Soliman M (2018) Geothermal exploration using airborne gravity and magnetic data at Siwa Oasis, Western Desert, Egypt. *Renew Sust Energ Rev* 82(3):3824–3832
- Abdelmaksoud A, El-Haddad E (2019) 2D inversion of refraction travel-time curves using homogeneous functions: a case study from Wadi El-Nakheil, Eastern Desert, Egypt. *Arab J Geosci* 12:214
- Abuzeid HI (1988) The youngest Precambrian volcanic succession of Wadi Hamrawein, Eastern desert, Egypt, PhD. Thesis., Earth Sc. And Res. Inst. South Carolina, Columbia, USA
- Affleck J (1963) Magnetic anomalies trend and spacing patterns. *Geophys.* 28(3):379–395
- Akaad S, Dardir A (1966) Geology of the Red Sea coast between Ras Shagara and Mersa Alam, Egypt. *Geol Surv Egypt* 35:67–79
- Akaad MK, El Ramly MF (1960) Geological history and classification of the basement rocks of the central eastern desert of Egypt. *Geol Surv Egypt* 9:1–24
- Akaad MK, Noweir A (1969) Lithostratigraphy of the Hammamat Um Seleimat district, Eastern Desert, Egypt. *Nature* 223:284–285
- Amer R, Ripperdan R, Wang T, Encarnación J (2012a) Groundwater quality and management in arid and semi-arid regions: case study, central Eastern Desert of Egypt. *J Afr Earth Sci* 69:13–25
- Amer R, Sultan M, Ripperdan R, Encarnacion J (2012b) Structural architecture for development of the marginal extensional sub-basins in the Red Sea active rift zone. *Int J Geosci* 3:133–152
- Amer R, Sultan M, Ripperdan R, Ghulam A, Kusky T (2013) An integrated approach for groundwater potential zoning in shallow fracture zone aquifers. *Int J Remote Sens* 34(19):6539–6561
- Andresen A, Abu El-Rus MA, Myhre PI, Boghdady GY, Corfu F (2008) U–Pb TIMS age constraints on the evolution of the Neoproterozoic Meatiq Gneiss Dome, Eastern Desert, Egypt. *Int J Earth Sci* 98:481–497. <https://doi.org/10.1007/s00531-007-0276-x>
- Atef H, Abd El-Gawad AMS, Abdel Zaher M, Farag KSI (2016) The contribution of gravity method in geothermal exploration of southern part of the Gulf of Suez–Sinai region, Egypt. *NRIAG J Astron Geophys* 5:173–185. <https://doi.org/10.1016/j.nrjag.2016.02.005>
- Ball J (1913) A brief note on the phosphate deposits of Egypt: Egypt Survey Dept., Cairo, 6 p
- Barron T, Hume WF (1902) Topography and geology of the Eastern Desert of Egypt (central portion): Egypt Geol Survey, Cairo, 331 p
- Beadnell HJL (1924) Report on the geology of the Red Sea coast between Quseir and Wadi Ranga: Petrol Res Bull, Gov 1 t. Press, Cairo, 37 p
- Chandrasekharan D, Lashin A, Al Arifi N, Al Bassam A, Singh HK (2016) Geothermal energy potential of eastern desert region, Egypt. *Environ Earth Sci* 75:697
- CONOCO (1987) Geological map of Egypt, scale 1: 500000, Sheet NG36NW-Quseir, Egypt. The Egyptian General Petroleum Corporation (EGPC), Cairo, Egypt
- El Shazly EM (1964) On the metallogenetic map of Egypt, Int. Geol. Congr. Rep., 22, India, New Delhi; Calcutta, 22, 418–425
- Elbarbary S, Abdel Zaher M, Mesbah H, El-Shahat A, Embaby A (2018) Curie point depth, heat flow and geothermal gradient maps of Egypt deduced from aeromagnetic data. *Renew Sust Energ Rev* 91:620–629
- El-Baz F (1995) Utilizing satellite images for ground water exploration in fracture zone aquifers. In Proceedings of the International Conference on water resources management in arid countries. Muscat, Oman, 2:419–427
- El-Gaby S, El Nady OM, Khudeir AA (1984) Tectonic evolution of the basement complex in the CED of Egypt. *Geol Rundsch* 73:1019–1036
- El-Gaby S, List FK, Tehrani R (1990) The basement complex of the Eastern Desert and Sinai. In: Said R (ed) *The Geology of Egypt*. A. A. Balkema, Rotterdam, pp 175–184
- El-Nouby MR, Ahmed EG (2007) Geothermal studies at Gebel El-Maghara area, North Sinai, Egypt. *Egypt Soc Environ Sci* 2(1): 23–32
- El-Ramly MF (1972) A new geological map for the basement rocks in the eastern and southwestern deserts of Egypt. *Egypt Geol Surv Ann* 2: 1–18
- El-Ramly MF, Budanov VI, Hussien AA, Dereniuk NE (1970) Ring complexes in the South Eastern Desert of Egypt, studies on some mineral deposits of Egypt, Nepheline Syenite project; part 3, *Geol Surv Egypt*, Cairo, Egypt, 81–194
- Faris MI, Hassan MY (1959) Report on the stratigraphy and fauna of the upper Cretaceous rocks of Um El Hueitat, Safaga area. *Bull Fac Sci Ain Shams Univ* 4:191–207
- Fowler AR, Ali KG, Omar SM, Eliwa H (2006) The significance of gneissic rocks and synmagmatic extensional ductile shear zones of the Barud area for the tectonics of the north Eastern Desert, Egypt. *J Afr Earth Sci* 46(3):201–220
- Fowler AR, Khamees H, Dowidar H (2007) El Sibai gneissic complex, Central Eastern Desert, Egypt: folded nappes and syn-kinematic gneissic granitoid sheets—not a core complex. *J Afr Earth Sci* 49(4):119–135
- Gaafar I, El-Shershaby A, Zeidan I, El-Ahll LS (2016) Natural radioactivity and radiation hazard assessment of phosphate mining, Quseir-Safaga area, Central Eastern Desert, Egypt, *NRIAG J Astron Geophys*
- Garson MS, Krs M (1976) Geophysical and geological evidence of the relationship of Red Sea transverse tectonics to ancient fractures. *Geol Soc Am Bull* 87(2):169–181
- Garson MS, Shalaby IM (1976) Precambrian-Lower Paleozoic plate tectonics and metallogenesis in the Red Sea region. *Geol Assoc Can Spec Pap* 14:573–596
- Gay SP Jr (1972): Fundamental characteristics of aeromagnetic lineaments, their geologic significance, and their significant to geology. “The new basement tectonics” American Stereo map Company, Salt Lake City, Utah., 94 P
- Ghanem MF, El-Fakharany MA, Temraz MG, Afife MM, Shehata AM (2016) Mineralogical and elemental compositions of oil shale in Duwi Formation Phosphate Mines, Safaga-Quseir Egypt, *Int J Innov Sci Eng Technol*, Vol. 3 Issue 2
- Gindy AR, Ghobrial WW, Badra EE (1973) Studied on Egyptian phosphates; I: thickness, phosphorous content, alpha radioactivity of the exploited phosphorite bed in Hamrawein area, Red Sea province, Egypt. *Proc Egypt Acad Sci* 26:1–17
- Gindy AR, Ghobrial WW, Badra EE (1976) Studied on Egyptian phosphates; II: intraphosphatic succession, mechanical analyses and

- radioactivity of the exploited phosphorite bed units in Hamrawein area, Red Sea province, Egypt. *Proc Egypt Acad Sci* 29:129–144
- Girdler RW, Evans TR (1977) Red Sea heat flow. *Geophys J R Astron Soc* 51:245–251
- Greene DC (1984) Structural geology of the Quseir area, Red Sea coast, Egypt: contribution no. 52 (M. S. Thesis), Department of Geology and Geography, University of Massachusetts, Amherst, 159 p
- Hall DH (1964) Magnetic and tectonic regionalization on Texada Island, British Columbia. *Geophysics* 29(4):566–308
- Hayba DO, Ingebritsen SE (1994) The computer model HYDROTHERM, A three-dimensional finite-difference model to simulate ground-water flow and heat transport in the temperature range of 0 to 1,200 °C: U.S. Geological Survey Water-Resources Investigations Report 94–4045, 85 p
- Heath R, Vanstone S, Swallow J, Ayyad M, Amin M, Huggins P et al. (1998) Renewed exploration in the offshore North Red Sea
- Hume WF (1935) The late plutonic and intrusive rocks, part 2: *Geol Surv Egypt*, 2, 301–688
- Issawi B, Francis M, El-Hennawy M, Mehanna A (1969) Contribution to the structure and phosphate deposits of Quseir area. *Geol Surv Egypt* 50:35
- Khalil SM, McClay KR (2001): Tectonic evolution of the NW Red Sea-Gulf of Suez rift system. In Wilson, R.C.L., Whitmarsh, R.B., Taylor, B. & Froitheim, N. Non-volcanic rifting of continental margins: a comparison of evidence from land and sea. Special Publication, no. 187. Geological Society of London. p. 453–473
- Khalil SM, McClay KR (2002) Extensional fault-related folding, north-western Red Sea, Egypt. *J Struct Geol* 24(4):743–762
- Khalil SM, McClay KR (2009) Structural control on syn-rift sedimentation, northwestern Red Sea margin, Egypt. *Mar Pet Geol* 26(6): 1018–1034
- Lashin A (2013) A preliminary study on the potential of the geothermal resources around the Gulf of Suez, Egypt. *Arab J Geosci* 6:2807–2828
- Lashin A (2015) Geothermal resources of Egypt, country update. In: *Proceedings World Geothermal Congress, Melbourne, Australia*, (13p)
- Martinez F, Cochran JR (1989) Geothermal measurements in the northern Red Sea: implications for lithospheric thermal structure and mode of extension during continental rifting. *JGR Solid Earth*. <https://doi.org/10.1029/JB094iB09p12239>
- MDA Federal (2004) Landsat GeoCover ETM+ 2000 Edition Mosaics (Tiles: N-35-25, N-35-30, N-36-25 and N-36-30. ETM-EarthSat-MrSID). USGS, Sioux Falls, South Dakota
- Meneisy MY (1990) Volcanicity, Chapt.9 In *Geology of Egypt*, (Said, R, Ed.), Balkema Pub. Rotterdam, Netherlands, pp.157–172
- Metawi MMA (2017) Geophysical data interpretation of Duwi area, central eastern desert of Egypt. M.Sc. Thesis. Faculty of Science, South Valley University, Egypt, 118p
- Miller HG, Singh V (1994) Potential field tilt – a new concept for location of potential sources. *Appl Geophys* 32:213–217
- Mohamed HS, Abdel Zaher M (2019) Subsurface structural features of the basement complex and geothermal resources using aeromagnetic data in the Bahariya Oasis, Western Desert, Egypt. *J Pure Appl Geophys* 177:2791–2802. <https://doi.org/10.1007/s00024-019-02369-z>
- Mohamed HS, Abdel Zaher M, Senosy MM, Saibi H, El Nouby M, Fairhead D (2015) Correlation of aerogravity and BHT data to develop a geothermal gradient map of the northern Western Desert of Egypt using an artificial neural network. *J Pure Appl Geophys* 172(6):1585–1597
- Montenant C, D'Estevou PO, Purser BH, Burrollet PF, Jarrige JJ, Orszag-Sperber F (1988) Tectonic and sedimentary evolution of the Gulf of Suez and the northwestern Red Sea. *Tectonophysics* 153(1–4):161–177
- Morgan P, Swanberg CA (1979) Heat flow and the geothermal potential of Egypt. *Pageoph* 117:213–226
- Morgan P, Boulos FK, Swanberg CA (1983) Regional geothermal exploration in Egypt. *Geophys Prospect* 31:361–376
- Morgan P, Boulos FK, Hennin SF, El-Sherif AA, El-Sayed AA, Basta NZ, Me-lek YS (1985) Heat flow in eastern Egypt: the thermal signature of a continental breakup. *J Geodyn* 4:107–131
- Moustafa AR (1997) Controls on the development and evolution of transfer zones: the influence of basement structure and sedimentary thickness in the Suez rift and Red Sea. *J Struct Geol* 19(6):755–768
- Oasis Montaj Programs (2014) Geosoft mapping and processing system: Version 8.3. (HJ), Inc Suit 500, Richmond St. West Toronto, ON Canada N5S1V6. <https://www.seequent.com/products-solutions/geosoft-oasis-montaj/>
- Parasnis DS (1986) Principles of applied geophysics, 4th edn. Chapman and Hall, London
- Ravat D, Salem A, Abdelaziz AMS, Elawady E, Morgan P (2011) Probing magnetic bottom and crustal temperature variations along the Red Sea margin of Egypt. *Tectonophysics* 510:337–344
- Rosenbach O (1953) A contribution to the computation of second derivative from gravity data. *Geophysics* 18:894–912
- Ruelleu S, Moreau F, Bour O, Gapais D, Martelet G (2010) Impact of gently dipping discontinuities on basement aquifer recharge: an example from Ploemeur (Brittany, France). *J Appl Geophys* 70:161–168
- Said R (1990) The geology of Egypt. Balkema, Rotterdam, p 734
- Saleh S, Salk M, Pamukcu O (2012) Estimating Curie point depth and heat flow map for northern Red Sea rift of Egypt and its surroundings, from aeromagnetic data. *Pure Appl Geophys* 170:863–885
- Salem A, Aboud E, Elsirafi A, Ushijima K (2005) Structural mapping of Quseir area, northern Red Sea, Egypt, using high-resolution aeromagnetic data. *Earth Planets Space* 57:761–765
- Salem A, Williams S, Fairhead JD, Ravat D, Smith R (2007) Tilt-depth method: A simple depth estimation method using first-order magnetic derivatives. *Lead Edge* 26:1502–1505
- Shalaby A, Stüwe K, Fritz H, Makroum F (2006) The El Mayah molasses basin in the Eastern Desert of Egypt. *J Afr Earth Sci* 45:1–15
- Sharma PV (1986) *Geophysical methods in geology*. 2nd Edn. Elsevier Scientific publishing Company, Amsterdam, p 442
- Sultan M, Wagdy A, Manocha N, Sauck W, Abdel GK, Youssef A, Becker R, Milewski A, El Alfy Z, Jones C (2008) An integrated approach for identifying aquifers in transcurrent fault systems: the Najd shear system of the Arabian Nubian shield. *J Hydrol* 349:475–488
- Sultan M, Youssef A, Metwally S, Becker R, Milewski A, Sauck W et al (2011) Red Sea rifting controls on aquifer distribution: constraints from geochemical, geophysical, and remote sensing data. *Geol Soc Am Bull* 123(5–6):911–924
- Swanberg CA, Morgan P, Boulos FK (1983) Geothermal potential of Egypt. *Tectonophysics* 96:77–94
- Swanberg CA, Morgan P, Boulos FK (1988) Geochemistry of the groundwaters of Egypt. *Ann Geol Surv* 14:127–150
- Telford WM, Gelbart LP, Sheriff RE, Keys DA (1990) *Applied geophysics*. Cambridge Univ., press, Cambridge, p 770
- Valentine MJ (1985) Structure and tectonics of the southern Gebel Duwi area, Eastern Desert of Egypt. Contribution no. 53, Department of Geology and Geography, University of Massachusetts, Amherst, 156p
- Younes A, McClay K (2001) Role of basement fabric on rift architecture: Gulf of Suez–Red Sea, Egypt. *Am Assoc Pet Geol Bull* 86:1003–1026
- Younes A, McClay K (2002) Development of accommodation zones in the Gulf of Suez-Red Sea Rift, Egypt. *AAPG Bull* 86(6):1003–1026
- Youssef MI (1957) Upper Cretaceous rocks in Kosseir area: *Bull Inst Desert Egypte*, v. 7, p. 35–53
- Youssef AM, Pradhan B, Gaber AFD, Buchroithner MF (2009) Geomorphological hazard analysis along the Egyptian Red Sea coast between Safaga and Quseir. *Nat Hazards Earth Syst Sci* 9: 751–766